Title
Determination of human skin optical properties from spectrophotometric measurements based on optimization by genetic algorithms

Journal
Journal of Biomedical Optics, 10(2)

ISSN
1083-3668

Authors
Zhang, Rong
Verkruysse, Wim
Choi, Bernard
et al.

Publication Date
2005

DOI
10.1117/1.1891147

Determination of human skin optical properties from spectrophotometric measurements based on optimization by genetic algorithms

Rong Zhang
Wim Verkruysse
Bernard Choi
University of California
Beckman Laser Institute
1002 Health Sciences Road East
Irvine, California 92612
E-mail: zhangr@uci.edu

John A. Viator
Oregon Health and Science University
Department of Dermatology
Portland, Oregon 97239

Byungjo Jung*
University of California
Beckman Laser Institute
1002 Health Sciences Road East
Irvine, California 92612

Lars O. Svaasand
Norwegian University of Science and Technology
NO-7491
Trondheim, Norway
and
University of California
Beckman Laser Institute
1002 Health Sciences Road East
Irvine, California 92612

Guillermo Aguilar
University of California
Beckman Laser Institute
1002 Health Sciences Road East
Irvine, California 92612
and
University of California
Department of Mechanical Engineering
Riverside, California 92521

J. Stuart Nelson
University of California
Beckman Laser Institute
1002 Health Sciences Road East
Irvine, California 92612

Abstract. We present an initial study on applying genetic algorithms (GA) to retrieve human skin optical properties using visual reflectance spectroscopy (VRS). A three-layered skin model consisting of 13 parameters is first used to simulate skin and, through an analytical model based on optical diffusion theory, we study their independent effects on the reflectance spectra. Based on a preliminary analysis, nine skin parameters are chosen to be fitted by GA. The fitting procedure is applied first on simulated reflectance spectra with added white noise, and then on measured spectra from normal and port wine stain (PWS) human skin. A normalized residue of less than 0.005 is achieved for simulated spectra. In the case of measured spectra from human skin, the normalized residue is less than 0.01. Comparisons between applying GA and manual iteration (MI) fitting show that GA performed much better than the MI fitting method and can easily distinguish melanin concentrations for different skin types. Furthermore, the GA approach can lead to a reasonable understanding of the blood volume fraction and other skin properties, provided that the applicability of the diffusion approximation is satisfied. [DOI: 10.1117/1.1891147]

Keywords: genetic algorithms; skin optical properties; visual reflectance spectrum; diffusion approximation; port wine stain.

Paper 04101 received Jun. 16, 2004; revised manuscript received Aug. 5, 2004; accepted for publication Sep. 9, 2004; published online Apr. 14, 2005.

1 Introduction

To assist the diagnosis and therapy of human skin pathology, objective assessment of skin characteristics is required. For example, in laser therapy of port wine stain (PWS) birthmarks, precise knowledge of skin characteristics such as epidermal thickness, epidermal melanin concentration, and blood vessel size, depth, and density will lead to the selection of optimal treatment parameters on an individual patient basis. Visible reflectance spectroscopy (VRS) is a widely used noninvasive measurement to determine the major chromophores of human skin,[1–3] and should be well suited to help guide the selection of optimal treatment parameters for PWS laser surgery.

Human skin shows great variation in optical properties on an individual patient basis and even from site to site on the same patient. However, skin has relatively homogeneous histological structures at certain depths, which allows it to be

*Current affiliation: Yonsei Univ., College of Health Sciences, Dept. of Biomedical Engineering, Korea.

1083-3668/2005/$22.00 © 2005 SPIE

investigated as a multilayered medium. A three-layered model, containing epidermal, normal, and PWS dermal layers, was developed by Svaasand et al.,[4] in which an optical diffusion approximation was used to fit manually measured reflectance spectra. Later, Douven and Lucassen[5] extended this three-layered skin model to a five-layered model containing epidermis, superficial plexus, dermis, deep blood plexus, and hypodermis. This model was used to obtain the scattering coefficient and blood volume fraction of each layer. Recently, a more detailed seven-layered model,[3] corresponding to a classic drawing by Spalteholz,[6] which contains stratum corneum, epidermis, papillary dermis, upper blood plexus, reticular dermis, deep blood plexus, and subcutaneous fat, was developed using a Monte Carlo method to simulate light distribution in human skin.

While different methods have been used to model skin, it is nevertheless generally agreed that color is mainly determined by melanin and hemoglobin concentrations.[7,8] In PWS skin, the visual appearance of the lesion is caused by the abnormally high density of blood in the subepidermis and upper dermal layers.[2,9]

Numerous methods have been developed to measure the optical properties of tissue. A detailed review by Cheong, Prahl, and Welch[10] compared three categories of methods for measuring and calculating scattering and absorption coefficients: direct, noniterative indirect, and iterative indirect methods. These authors suggested that iterative methods have the advantage of utilizing complicated mathematical expressions and, thus, lead to more accurate solutions. Therefore, in the present work, we use an iterative procedure to analyze measurements obtained with VRS.

Several authors have suggested multiple approaches to estimate skin parameters from measured diffuse reflectance spectra. Matcher[11] used a multilinear regression (MLR) method; however, it has been reported that the MLR method might have overfitting problems.[12] Farrell, Wilson, and Patterson[13] used a neural network (NN) method to determine tissue optical properties from spatially resolved diffuse reflectance measurements; however, for NN to have training sets that can initially ''teach the neurons,'' a number of accurate correlations between skin parameters and VRS measurements are required. The best way to achieve this is through skin biopsies, so this approach is rejected for the current study of noninvasive methods. Douven and Lucassen[5] used a Simplex optimization method[14]; however, it has been reported that the Simplex method is more suitable for local optimization problems.[15] We expect that the solution space of the current problem is very complex, so that a local optimization method would be of limited use.

A GA approach was first developed by Holland.[16] GA is a stochastic method based on Darwin's evolution hypothesis of survival of the fittest. Because of its reliable global convergence properties, GAs have been widely used in solving optimization problems. To our knowledge, this is the first study that applies a GA for the determination of skin optical properties from measurements obtained with VRS. The aim of this work is to introduce the approach of combining GA and VRS measurements to retrieve skin properties, and thus assist clinical treatment and diagnosis.

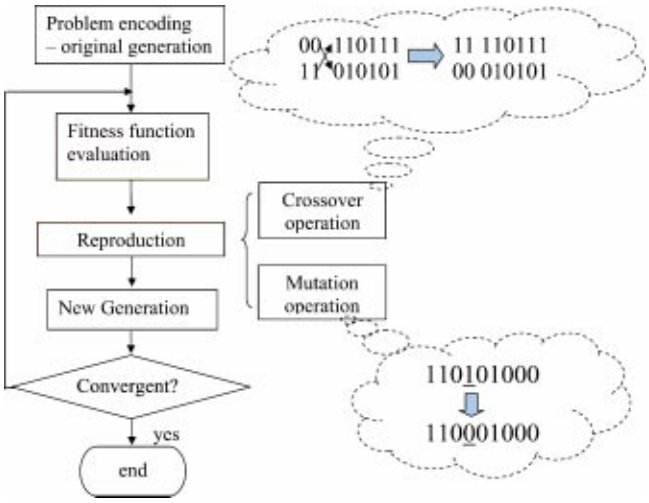

Fig. 1 Flowchart of a GA and examples of crossover and mutation operations.

2 Methods

2.1 *Genetic Algorithms*

A standard GA consists of problem encoding, fitness function evaluation, crossover operation, and mutation operation.[16,17] A flow chart is shown in Fig. 1. For the application of GAs to the topic under study, the iterative algorithm is performed as follows.

1. Problem encoding: The search for optimal fitting parameters starts by randomly generating a population of n parameter sets, within their reasonable ranges. Each set of parameters is then encoded into a binary string known as the ''chromosome.''
2. Fitness function evaluation: The fitness function, which is the normalized residue, is compared within each generation (i.e., iteration of the GA). The chromosomes are ranked in order from the smallest residues to the largest. Half of the chromosomes with the smallest residues are preserved to become the parent chromosomes for the next generation.
3. Reproduction: To replace the discarded chromosomes and to avoid entrapment into a local minima in the solution space, new chromosomes, called offspring, are introduced by the so-called crossover operation and mutation operation, as illustrated in Fig. 1.

By repeating steps 2. and 3. in an iterative fashion, the GA converges toward the optimal chromosome.

The convergence time is related to both the number of parameter sets in one population (n) and number of iteration steps (N). Greater n and N will improve the likelihood of convergence but will require longer computation times. After trying different combinations of n and N for the current problem, we decided to use a small population ($n=8$) of randomized initial chromosomes; simultaneously, to avoid being trapped by ''bad parent genes,'' we allowed the algorithm to restart ten times after every 300 iterations. The best result was selected from the fitted spectra produced over these ten runs.

The advantage of GAs is that randomizing the initial start-

ing chromosomes permits exploration of the entire solution space, and thus serves as a powerful tool to find a global, rather than a local, optimum.

2.2 *Analytical Model*

Ideally, GAs may be used to optimize any computational method. However, numerical methods such as Monte Carlo simulations[18] when used conventionally are very time consuming and computationally intense to be incorporated into iterative optimization loops. Recently, Spanier and coworkers have developed adaptive Monte Carlo (MC) methods[19–21] that dramatically increased the rate of convergence of simulation for transport problems. However, even these improved MC algorithms will require at least several minutes to compute one spectrum over the entire visible wavelength range. In the present work, we adapted an analytical model based on an optical diffusion approximation detailed in the thesis of Keijzer.[22]

2.3 *Selection of Parameters*

It is necessary to decide how many skin layers should be modeled and which parameters should be included in the optimization algorithm. Since some skin parameters are strongly interdependent, it is very difficult to describe mathematically the interdependency between parameters; on the other hand, it is also impractical to include all the parameters into the fitting procedure, which will cause nonuniqueness of the solution space.

We first established a five-layered model according to Douven and Lucassen.[5] Each layer is characterized by parameters describing the optical properties and morphology. Then we set out to reduce the number of parameters to be optimized by determining the relative impact of each parameter on the visual reflectance spectrum. For example, to determine the impact of the papillary upper dermal thickness ($z2$), we set all other parameters constant at their average values, and varied $z2$ by $\pm 30\%$.[3] For all $z2$ values, we then plotted the reflectance spectra and compared them quantitatively. Since there were only slight offsets ($\sim \pm 0.7\%$) appearing in the 600- to 800-nm wavelength range, we decided to set $z2$ as a constant throughout the optimization process. By performing this procedure with each parameter, and assuming $\pm 1\%$ as the threshold maximum offset, we concluded the following.

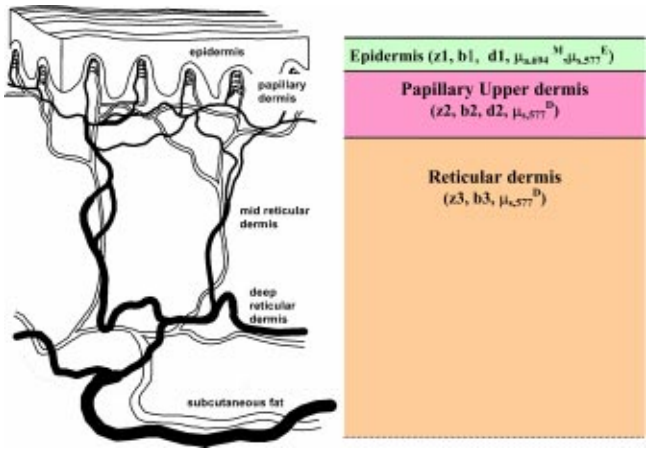

Fig. 2 Three-layered skin model used in the current study, symbols corresponding to Table 1. (Schematic courtesy of Wim Verkruysse, PhD thesis, 1998.)

1. For VRS, there is virtually no advantage in using a five-layered skin model that includes the deep blood plexus and subcutaneous fat as the fourth and fifth layers, respectively. Within reasonable parameter ranges collected from the literature,[2–4,7,23–28] the parameters for the fourth and fifth layers have a negligible effect on VRS. This conclusion agrees with that previously reported in the literature. Lakmaker, Pickering, and van Gemert[29] reported that the maximal depth at which ectatic blood vessels contribute to the abnormal PWS skin color is 0.9 mm for a normally pigmented epidermis and 0.8 mm for a darker pigmented epidermis. Also, Niechajev and Clodius[30] reported histological analysis on 50 PWS, which showed that PWS blood vessels in the deeper

Table 1 Parameters used in the fitting procedure (* are parameters to be fitted by the optimization routine).

Absorption coefficient of melanin at 694 nm ($\mu_{a,694}^{M}$)*	0.2 to 2.5 mm^{-1} (Caucasian: 0.2 to 0.3 mm^{-1}; Asian: 0.3 to 1.2 mm^{-1}; African: 2 to 2.5 mm^{-1})
Scattering coefficient of first layer ($\mu_{s,577}^{E}$)*	35 to 80 mm^{-1}
Scattering coefficient of second and third layer ($\mu_{s,577}^{D}$)*	10 to 50 mm^{-1}
Blood in first layer (b1)	0.2%
Blood in second layer (b2)*	Normal: 1 to 10%
	PWS: 5 to 30%
Blood in third layer (b3)*	Normal: 1 to 10%
	PWS: 1 to 20%
Thickness of first layer (z1)*	0.05 to 0.13 mm
Thickness of second layer (z2)	0.23 mm
Thickness of third layer (z3)	∞
Vessel diameter in first layer (d1)	0.008 mm
Vessel diameter in second layer (d2)*	Normal: 0.008 to 0.03 mm
	PWS: 0.02 to 0.2 mm
Oxygen saturation (SaOxy)*	50 to 100%
Hematocrit (H)*	Female: 36.1 to 44.3%
	Male: 40.7 to 50.3%

fourth and fifth layers were virtually nonexistent. Therefore, in the present study, we use a three-layered skin model as shown in Fig. 2. (The Maple® code for solving the optical diffusion equation and the Matlab® code for calculating the wavelength-dependent visual reflectance spectrum based on given skin properties are available for download from the website in Ref. 31).

2. The epidermal thickness ($z1$) and blood volume fraction in the first layer ($b1$) are strongly interdependent; use of both parameters as optimization targets will cause nonuniqueness to the solution. Therefore, we chose not to vary these two parameters simultaneously. In this study, we allowed $z1$ to be varied and set the epidermal blood volume fraction as a constant, i.e., $b1=0.2\%$,[4] to account for the few vessels protruding from the upper dermal papillary loops into the first planar layer with thickness $z1$.

3. Douven and Lucassen[5] selected the average blood vessel diameter in each layer as constant average values of normal skin (8, 12, and 30 μm for capillaries, superficial plexus, and dermis, respectively). In PWS skin, the average vessel diameter in the upper dermis was reported in the range of 10 to 50 μm after 3-D reconstruction of PWS anatomy using a series of histological sections.[32] A PWS blood vessel diameter of 10 to 200 μm was also reported by Svaasand et al.[4] Since vessel diameter significantly influences light absorption[33] and laser treatment response,[34] we chose the average vessel diameter (specifically, the blood vessel diameter in the second layer, $d2$) as one of the parameters to be fitted by our algorithms. In summary, we selected nine parameters to be included in the optimization routine, and set the remaining parameters at constant values as listed in Table 1.

2.4 *Implementation*

The diffusion model was programmed as a Matlab® function. The GA was programmed as an optimization tool using Matlab®.

To focus on fitting the reflectance spectra local minima in the wavelength regions of 500 to 600 and 680 to 780 nm, higher sampling (i.e., one sample per 2.2 nm) was used in these regions, while less sampling (i.e., one sample per 4.4 nm) was used elsewhere. Similarly, when there were similar residues achieved among fitting curves resulting from ten GA runs, we selected the one with the best fit in the wavelength regions of 500 to 600 and 680 to 780 nm. The normalized residue was chosen to be the fitness function in the optimization procedure:

$$R=\left\{\sum_{s=1}^{n}\frac{(\lambda_{s2}-\lambda_{s1})\Sigma_{\lambda=\lambda_{s1}}^{\lambda_{s2}}[m(\lambda)-f(\lambda)]^2}{N_s}\Big/\sum_{s=1}^{n}N_s\right\}^{1/2}, \quad (1)$$

where $m(\lambda)$ is the measured reflectance at wavelength λ, $f(\lambda)$ is the fitted reflectance at wavelength λ, and N_s is the number of samplings made in each wavelength section between λ_{s1} and λ_{s2}.

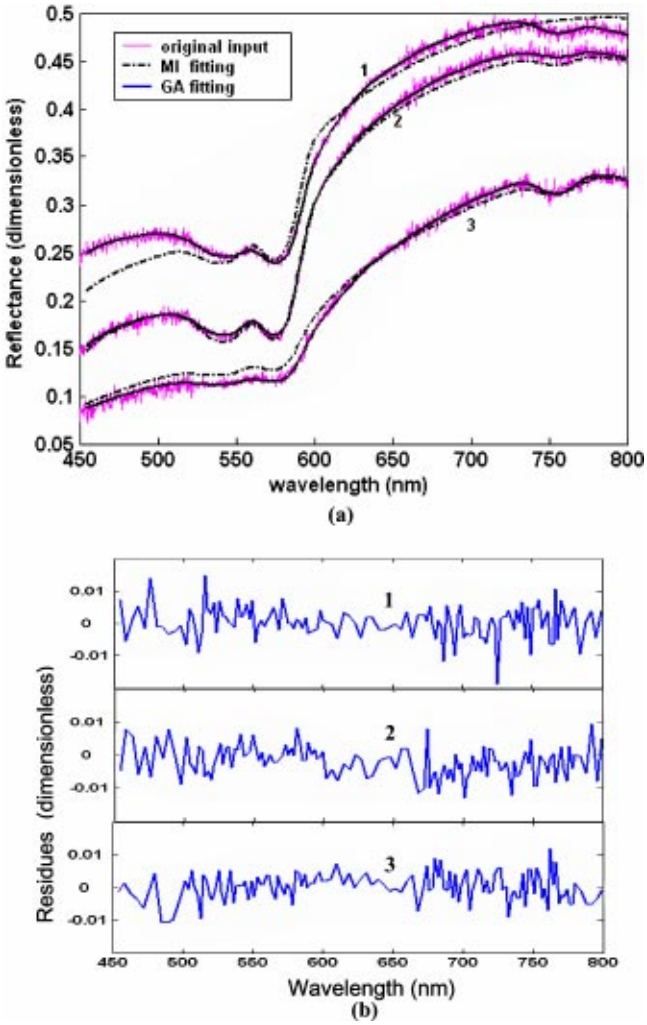

Fig. 3 (a) Comparison of fitting three simulated spectra with added white noise using GA and MI methods: the fitted spectra by using GA overlap with the original input spectra very well, while the fitted spectra by using MI have much larger residues. (Retrieved skin parameters corresponding to Table 2.) (b) Residues between simulated and fitted spectra using the GA method, the ranges of residues are at the same magnitude of added white noise.

3 Experimental Results

3.1 *Fitting Simulated Spectra*

To test our method, simulated spectra obtained from forward calculation based on known parameters were used as input into the GA. Three sets of parameters were used to simulate three noticeably different spectra representative of normal and PWS human skin [Fig. 3(a)]. To simulate the same noise amplitudes as in our measurements where substantial noise was observed at relatively short and long wavelengths, white noise with amplitudes of ± 0.01 and ± 0.02 was added to the calculated spectrum at wavelengths of 520 to 650 nm and at all other wavelengths, respectively.

Using the GA, all nine parameters were fitted simultaneously for each spectrum. The ranges of the initial parameters were chosen as same as those listed in Table 1. The smooth solid lines in Fig. 3(a) indicate the best fits after applying the GA. Figure 3(b) shows the residues between the

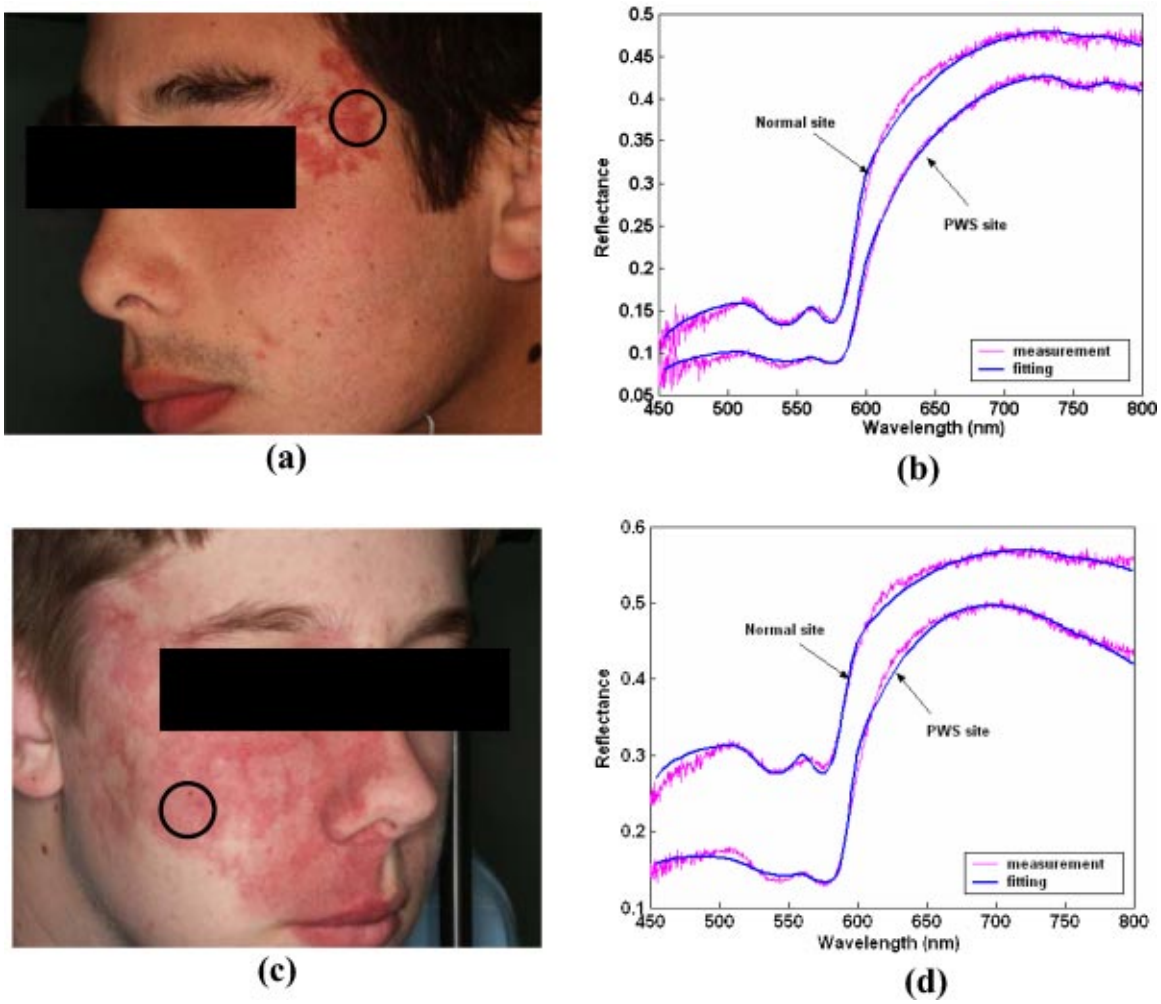

Fig. 4 Photo and GA fitting results of VRS measurements on normal and PWS sites from: (a) and (b) Asian male with a dark red PWS, and (c) and (d) Caucasian male with a light pink PWS. The GA approach can distinguish between different skin types, it can also distinguish skin parameters between normal and PWS skin. [Note: black circles in (a) and (c) indicate the sites where measurements were taken. Retrieved parameters correspond to Table 5.]

simulated and fitted spectra after using the GA. It can be noted that the ranges of residues are at the same magnitude as the added white noise.

For comparison, one of our authors, who has extensive experience with manual fitting of VRS measurements,[35] tried to fit the same three curves without any knowledge of the input parameters. He used a simple manual iteration (MI) method, which is to vary each parameter independently and then optimize them one by one. The dashed lines in Fig. 3(a) present the best fits obtained from MI. It can be noted that the residues are much larger.

Tables 2, 3, and 4 list the original inputs, fitted parameters, and their differences for the three simulated curves using the two fitting methods. Note that when using the GA, although vessel radii sometimes (as in Tables 2 and 4, line 8) have greater than 30% errors, the relative errors of all other parameters are below 20%. When using MI, even with some known parameters, the errors are much larger. Thus, we concluded that GA performed much better than MI for fitting spectra.

The computation time used for a GA with 300 generations is 30 s on a Pentium® 4 computer with 2.6-GHz CPU. Therefore, it takes 5 min of computer time to fit one curve, since the algorithm is allowed to restart ten times. In comparison, MI requires 20 to 40 min of combined computer time and constant human participation.

3.2 *Fitting Measured Spectra*

3.2.1 *Comparison between normal and PWS sites*

Our measurements were conducted using instruments from Ocean Optics Incorporated (Dunedin, Florida): spectrometer (SD2000), integrating sphere (ISP-REF, 10-mm aperture), fiber optic variable attenuator (FVA-UV), and diffuse reflectance standards (Labsphere Incorporated, North Sutton, New Hampshire) for calibration. A notebook computer (Presario 2500, Compaq) was used for data acquisition.

Measurements were acquired from two patients with PWS skin. Patient A [Fig. 4(a)] is an Asian male with a dark red PWS on the left upper cheek. Patient B [Fig. 4(c)] is a Caucasian male with a light pink PWS on the right upper lip and cheek. All photos presented in this work were acquired with a standardized cross-polarized digital imaging system.

Table 2 Comparison of using GA and MI to fit simulated spectra (input 1) with added white noise.

		Input 1	Using GA fitted data	Error	Using MI fitted data	Error
1	Residue		0.0047		0.0163	
2	$\mu_{a,694}^{M}$ (mm^{-1})	0.25	0.23	–8.0%	0.4	60.0%
3	$\mu_{s,577}^{E}$ (mm^{-1})	60	56.2	–6.3%	60	0.0%
4	$\mu_{s,577}^{D}$ (mm^{-1})	30	33	10.0%	30 known)	—
5	b2 (%)	15.0	15.3	2.0%	5	–66.7%
6	b3 (%)	6	7.1	18.3%	3	–50.0%
7	z1 (mm)	0.1	0.11	10.0%	0.1 (known)	—
8	d2 (mm)	0.04	0.026	–35.0%	0.020	–50.0%
9	SaOxy (%)	80	80	0.0%	99	23.8%
10	Hematocrit (%)	42	43.2	2.9%	42 (known)	—

Table 3 Comparison of using GA and MI to fit simulated spectra (input 2) with added white noise.

		Input 2	Using GA fitted data	Error	Using MI fitted data	Error
1	Residue		0.0049		0.0076	
2	$\mu_{a,694}^{M}$ (mm^{-1})	0.5	0.59	18.0%	0.3	–40.0%
3	$\mu_{s,577}^{E}$ (mm^{-1})	50	58.6	17.2%	27	–46.0%
4	$\mu_{s,577}^{D}$ (mm^{-1})	30	31	3.3%	25	–16.7%
5	b2 (%)	8	8.4	5.0%	5	–37.5%
6	b3 (%)	6	6.5	8.3%	6 (known)	—
7	z1 (mm)	0.07	0.06	–14.3%	0.1	42.9%
8	d2 (mm)	0.02	0.016	–20.0%	0.02 (known)	—
9	SaOxy (%)	85	86	1.2%	80	–5.9%
10	Hematocrit (%)	48	45.8	–4.6%	42	–12.5%

Table 4 Comparison of using GA and MI to fit simulated spectra (input 3) with added white noise.

		Input 3	Using GA fitted data	Error	Using MI fitted data	Error
1	Residue		0.0042		0.0087	
2	$\mu_{a,694}^{M}$ (mm^{-1})	0.7	0.77	10.0%	0.4	–42.9%
3	$\mu_{s,577}^{E}$ (mm^{-1})	40	45.5	13.8%	25	–37.5%
4	$\mu_{s,577}^{D}$ (mm^{-1})	25	28.1	12.4%	20	–20.0%
5	b2 (%)	25	28.1	12.4%	12	–52.0%
6	b3 (%)	15	17	13.3%	13	–13.3%
7	z1 (mm)	0.11	0.1	–9.1%	0.2	81.8%
8	d2 (mm)	0.06	0.04	–33.3%	0.020	–66.7%
9	SaOxy (%)	75	70	–6.7%	70	–6.7%
10	Hematocrit (%)	40	40.4	1.0%	42	5.0%

Table 5 Fitting results of VRS measurements on normal and PWS sites from two patients.

		Patient A		Patient B	
		Normal	PWS	Normal	PWS
1	Residue	0.0068	0.0041	0.0081	0.007
2	$\mu_{a,694}^{M}$ (mm^{-1})	0.67	0.74	0.25	0.25
3	$\mu_{s,577}^{E}$ (mm^{-1})	42.9	40.7	45.5	35.6
4	$\mu_{s,577}^{D}$ (mm^{-1})	43.1	36.9	49.8	32.4
5	b2 (%)	8.8	28.2	3.4	22.2
6	b3 (%)	9.3	6.8	9.8	10.4
7	z1 (mm)	0.051	0.050	0.057	0.053
8	d2 (mm)	0.024	0.080	0.028	0.106
9	SaOxy (%)	93.2	84.6	94.6	97.5
10	Hematocrit (%)	48	45	44	46

Measurements of VRS were taken on both PWS and adjacent normal skin sites. For each measurement, the contact pressure between the integrating sphere and the skin was kept as constant as possible. Three to five measurements were taken at each site to ensure good repeatability. The averages of all measurements were calculated and used for fitting. The fitted and the averages of measured curves were plotted in Figs. 4(b) and 4(d) for patients A and B, respectively. From the numerical results listed in Table 5, it can be concluded that:

1. patient A (Asian) has a higher melanin absorption coefficient ($\mu_{a,694}^{M}$) than patient B (Caucasian), as shown in Table 5, line 2
2. both patients have a considerably higher blood volume fraction in the upper dermal layer (b2) on PWS as compared to normal skin (Table 5, line 5)
3. both patients have an average blood vessel diameter (d2) on PWS sites that is greater than that from normal sites (Table 5, line 8), even taking into account the $\pm 30\%$ error margin as calculated from fitting the simulated spectra (Tables 2 and 4, line 8).

3.2.2 *Comparison of three different PWS sites*

Figure 5 shows photos and fitting results of measured reflectance spectra for three PWS patients with different lesion colors on different anatomical locations. All three patients are Caucasian. Patient 1 [Fig. 5(a)] has a light pink PWS unevenly distributed over his face; patient 2 [Fig. 5(c)] has a red PWS evenly distributed on his forearm; and patient 3 [Fig. 5(e)] has a red PWS under her left eye. The fitted and the averages of the measured curves were plotted in Figs. 5(b), 5(d), and 5(f) for patients 1, 2, and 3, respectively. Table 6 summarizes the results.

1. Patients 1, 2, and 3 have the lowest, intermediate, and highest blood volume fractions, respectively. This is true for the second (b2) and third layers (b3), as in Table 6, lines 5 and 6
2. The average blood vessel diameter (d2) of patients 2 and 3 are both greater than those of patient 1 (Table 6, line 8).
3. Comparing the melanin absorption coefficients ($\mu_{a,694}^{M}$) from these three patients (Table 6, line 2) with patient A (Table 5, line 2), it appears that Caucasians have lower $\mu_{a,694}^{M}$ values than Asians.

4 Discussion

In this study, the optical diffusion approximation and a layered skin structure were used to model human skin. By using GA, nine optical and structural properties of the skin were simultaneously extracted from each reflectance spectrum. Comparisons between applying GA and MI fitting showed that the approach under study performed much better than the MI fitting method. The GA approach can easily distinguish melanin concentrations for patients with different skin types while also leading to a reasonable understanding of the blood volume fraction and other skin properties.

It is notable that our fits to the measured spectra did not agree as well as those to simulated spectra. The former tended to result in higher than realistic values for blood volume fraction (b2, b3) and oxygen saturation (SaOxy). These results may be explained by the following.

4.1 *Possible Modeling Errors*

1. The diffusion approximation is only valid in the case of light transport when the medium is dominated by scattering, i.e., the inequality $\mu_a/\mu_s(1-g) \ll 1$ must be satisfied[36] for each of the three layers in the skin model. Figure 6 illustrates the calculation of $\mu_a/\mu_s(1-g)$ corresponding to the three PWS sites of patients 1, 2, and 3 [Figs. 6(b), 6(c), and 6(d)]. For comparison, the validity condition for patient 1 normal skin site was also plotted [Fig. 6(a)]. We found that the diffusion approximation was pushed to its limit for the mathematical model to be able to fit the high blood volume fraction at the PWS sites. For example, for patient 1, the maximum value of $\mu_a/\mu_s(1-g)$ in the second layer reaches 0.8 [Fig. 6(b)], and for patient 3, the maximum value in the third layer is greater than unity [Fig. 6(d)]. Therefore, the diffusion approximation is no longer valid and the absolute values of parameters obtained from the curve fitting are inaccurate and the only conclusion that can be drawn is that there tends to be more blood in patient 3's dermal layers. Determination of exactly how much more blood is beyond the limits of the present analytical model using diffusion approximation theory.

2. Douven and Lucassen[5] compared Keijzer's[22] diffusion approximation model with the Monte Carlo method, which is widely accepted as the most accurate simulation method. They found that in the case of diffuse illumination, the Keijzer model slightly underpredicts the Monte Carlo results over the entire wavelength range.

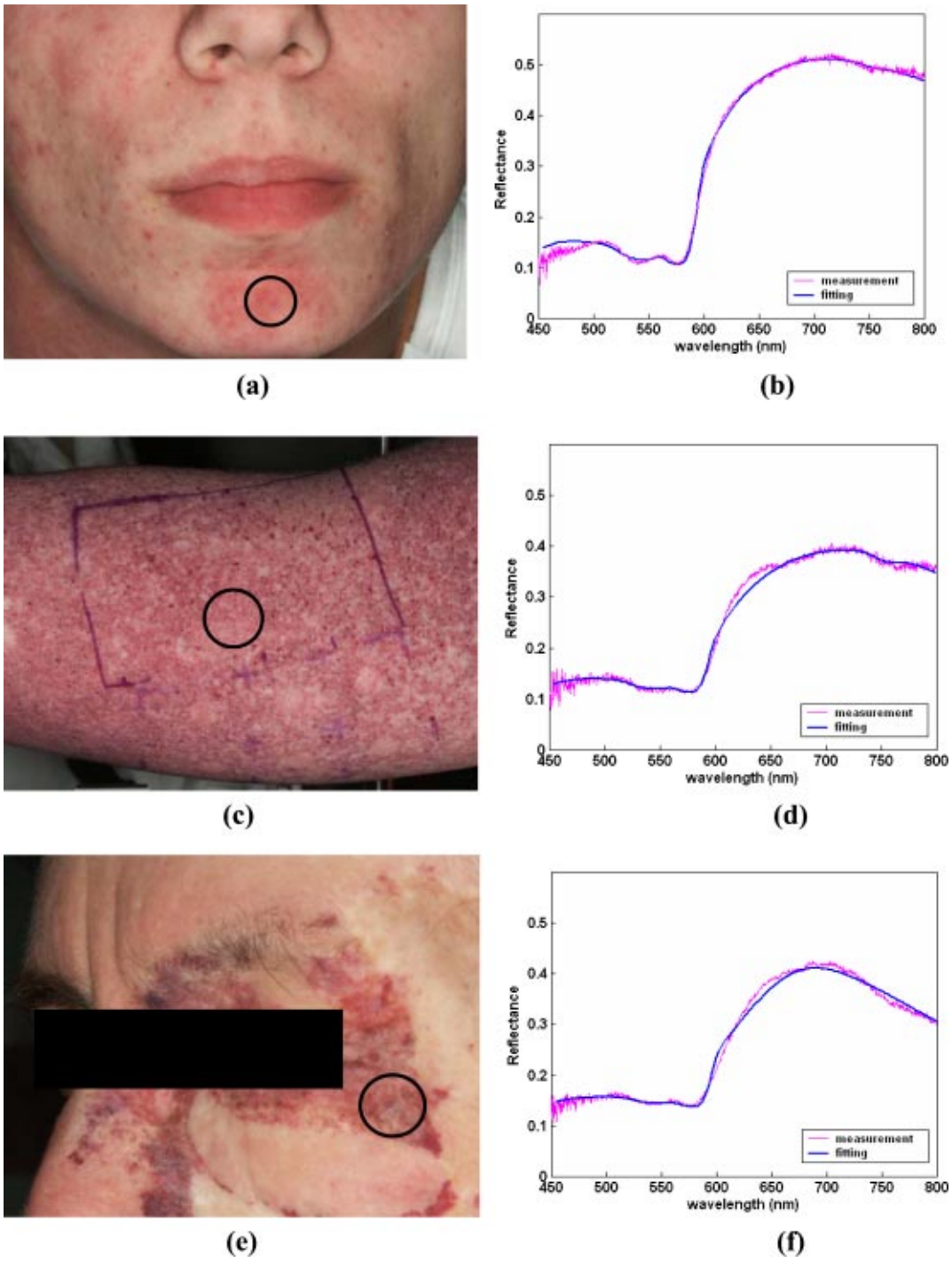

Fig. 5 Fitting results of VRS measurements on three PWS patients with different lesion colors on different anatomical locations. The GA approach can distinguish skin parameters for different lesions. [Note: black circles in (a), (c), and (e) indicate the sites where measurements were taken. Retrieved skin parameters correspond to Table 6.]

3. The adoption of the layered skin structure and the assumption that each layer is a homogeneous flat medium containing vessels of the same diameter are rough approximations.

4.2 *Possible Instrumentation Limitations*

1. The finite aperture of the integrating sphere results in loss of light in the wavelength range of 650 to 800 nm, leading to a reduction in the reflectance values. Considering that oxygen saturation is the only parameter under study that can cause a steep reduction of the reflectance spectrum at these wavelengths,[37] this may explain why an abnormally high oxygen saturation was retrieved.

2. With our measurement system, noise in the wavelength range of 800 to 1200 nm makes it impossible to utilize the information contained in those signals. Instrumentation that

Table 6 Fitting results of VRS measurements on three PWS patients with different lesion colors on different anatomical locations.

		Patient 1	Patient 2	Patient 3
1	Residue	0.0082	0.0075	0.0083
2	$\mu_{a,694}^{M}$ (mm^{-1})	0.27	0.23	0.33
3	$\mu_{s,577}^{E}$ (mm^{-1})	38.6	37.4	39.6
4	$\mu_{s,577}^{D}$ (mm^{-1})	35.7	31.6	29.6
5	b2 (%)	26	29	38
6	b3 (%)	3	17	28
7	z1 (mm)	0.058	0.052	0.093
8	d2 (mm)	0.052	0.096	0.094
9	SaOxy (%)	95	87	99
10	Hematocrit (%)	47	43	44

gives a clearer signal at a wider spectrum would be helpful.

4.3 *Parameter Selection*

Parameter selection was based on published literature, which gave quite different models for calculating skin optical properties.

1. Three different values or expressions of the baseline tissue absorption coefficient (μ_a^T) were reported. Douven and Lucassen[5] chose μ_a^T as a constant to be fitted, and reported values of 0.0158 and 0.0134 mm^{-1}, which are much lower values than the 0.025 mm^{-1} for the wavelength range of 600 to 900 nm used by Duck[38] and Svaasand.[4] In our study, we adopted the expression of wavelength-dependent μ_a^T,[39,40] i.e., $\mu_a^T = 7.84\times10^7\times\lambda^{-3.255}\,mm^{-1}$, to agree with other wavelength-dependent coefficients used in Keijzer's model.[5,22]

2. For skin melanosomes, Jacques[40] used $\mu_a^{melanosome} = 1.7\times10^{11}\times\lambda^{-3.48}\,mm^{-1}$, while the average melanin absorption coefficient of human skin given by Meglinski and Matcher[3] was $\mu_a^{melanin} = 5\times10^9\times\lambda^{-3.33}\,mm^{-1}$, and Svaasand et al.[4] used the average absorption coefficient at $\lambda = 694$ nm, $\mu_a^{melanin} = \mu_{a,694}^{melanin}(694/\lambda)$.[4]

In consideration of the previous, it is incorrect to use the numerical values obtained from the fitting algorithm as the actual quantities of the optical properties of human skin. However, the approach of combining VRS with GA is very useful to give a qualitative comparison of some skin features between different patients/sites, or on the same patient/site during different stages of treatment. VRS may be a valuable

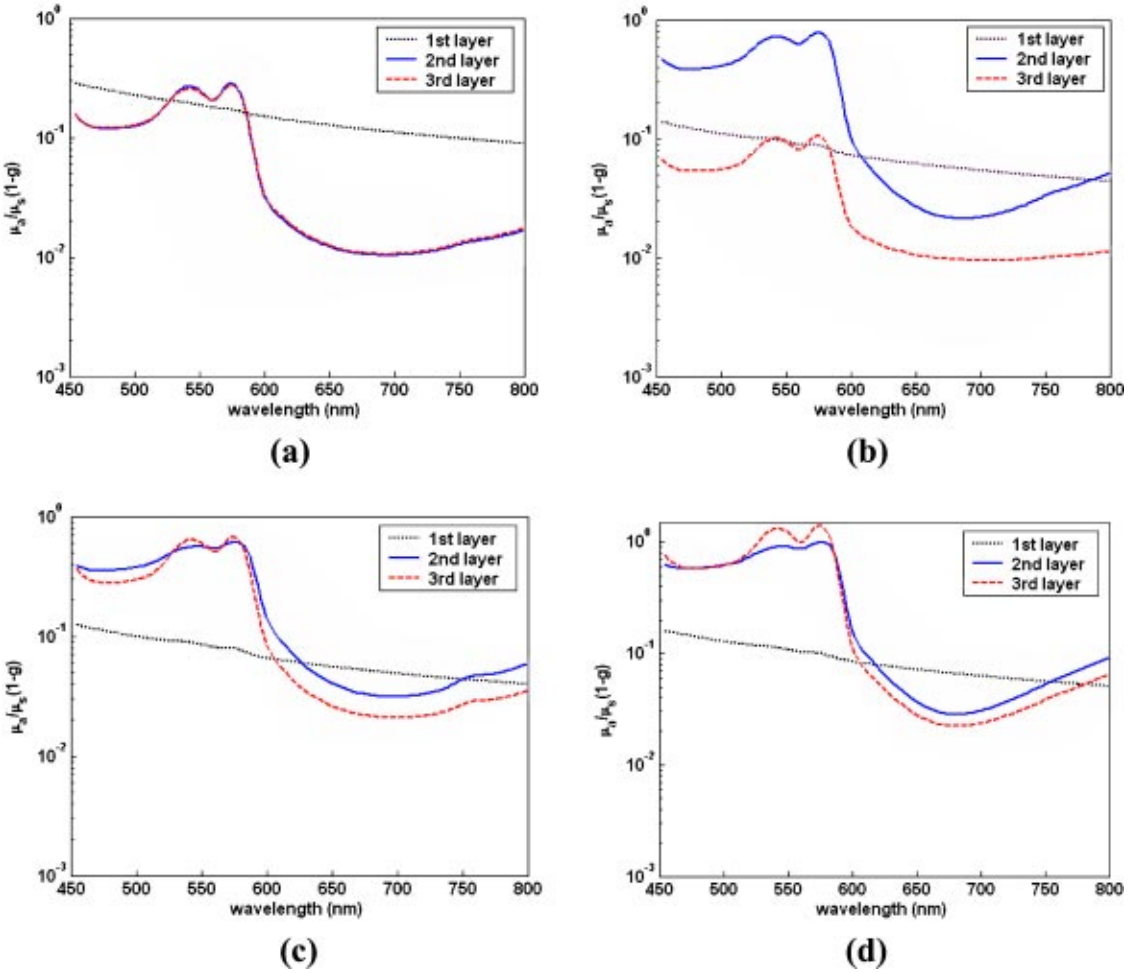

Fig. 6 Diffusion approximation validity condition for (a) patient A normal site, (b) patient 1 PWS site, (c) patient 2 PWS site, and (d) patient 3 PWS site. This condition is pushed to its limit for the case of high blood volume fraction at the PWS sites.

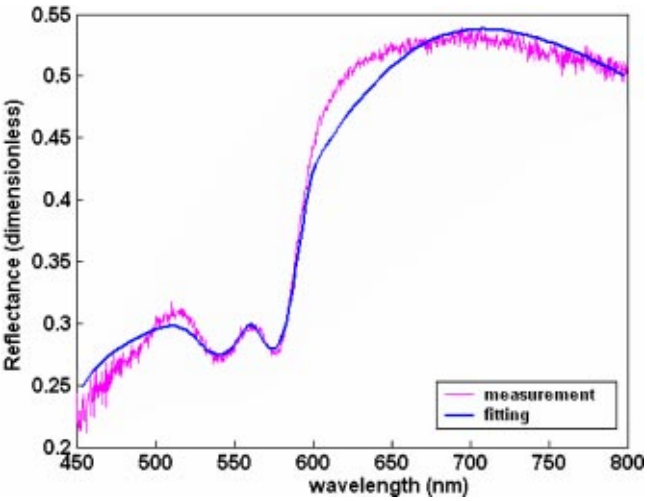

Fig. 7 Measured and GA fitted VRS on a normal skin site of a male Caucasian. The differentiation between the wavelengths 600 to 650 nm is not represented by the fitted spectrum (retrieved skin parameters correspond to Table 7.)

tool to monitor treatment response when used in conjunction with a diffusion theory-based model.

We believe that the time required for curve fitting can be further reduced by: 1. using hybrid optimization methods, e.g., combining GA with some local minimization methods, such as a Simplex algorithm[15]; and 2. providing more specific information about the patient under study, such as skin type and PWS color, before starting the fitting procedure. Thus, the range of certain fitting parameters, such as melanin absorption and blood volume fraction, can be reduced and constrained throughout the fitting algorithms.

An as yet unsolved problem is that we find that some measured VRS, specifically those of normal Caucasian skin, are very difficult to fit. Figure 7 shows a typical fitting result from a measurement done on the forearm of a 35-year-old Caucasian male. We arbitrarily enlarged the range of each fitting parameter (as in Table 7), but the differentiation between the wavelengths 600 to 650 nm is not represented by the fitted spectrum. One possible explanation is that the skin model is too simple to include all of the absorbing and scattering factors within human skin, particularly at some wavelengths.

Table 7 Fitting results of VRS measurement on normal Caucasian skin.

1	Residue	0.0138
2	$\mu_{a,694}^{M}$ (0.1 to 1.2 mm^{-1})	0.28
3	$\mu_{s,577}^{E}$ (30 to 80 mm^{-1})	41.6
4	$\mu_{s,577}^{D}$ (10 to 50 mm^{-1})	40.0
5	b2 (1 to 40%)	2
6	b3 (2 to 10%)	8
7	z1 (0.05 to 0.13 mm)	0.052
8	d2 (0.02 to 0.2 mm)	0.03
9	SaOxy (50 to 100%)	96
10	Hematocrit (40 to 50%)	49

5 Conclusions

We present an initial study using GA to retrieve human skin optical properties from measured VRS. The diffusion approximation and a layered skin structure are used to model human skin. Nine optical and structural skin properties are simultaneously extracted from each reflectance spectrum. A normalized residue of less than 0.005 was achieved for simulated spectra. In the case of measured spectra from human skin, the normalized residue is less than 0.01. Comparisons between applying GA and MI fitting show that the approach under study performs much better than the MI fitting method and can easily distinguish melanin concentrations for different skin types. Furthermore, the GA approach can lead to a reasonable understanding of the blood volume fraction and other skin properties, provided that the applicability of the diffusion approximation is satisfied.

Acknowledgments

BC acknowledges funding support from the Beckman Fellows Program. This study was funded by research grants from the National Institute of Health (GM62177, AR47551, AR48458 to JSN and HD42057 to GA).

References

1. E. Berardesca, P. H. Andersen, P. Bjerring, and H. I. Maibach, ''Erythema induced by organic-solvents—in vivo evaluation of oxygenized and deoxygenized hemoglobin by reflectance spectroscopy,'' *Contact Dermatitis* **27**, 8–11 (1992).
2. L. T. Norvang, E. J. Fiskerstrand, B. Badden, D. Grini, Ø. Standahl, T. E. Milner, M. W. Berns, J. S. Nelson, and L. O. Svaasand, ''The influence of tissue parameters on visual reflectance spectra of port-wine stains and normal skin,'' *Proc. SPIE* **2623**, 2–14 (1995).
3. I. V. Meglinski and S. J. Matcher, ''Quantitative assessment of skin layers absorption and skin reflectance spectra simulation in the visible and near-infrared spectral regions,'' *Physiol. Meas* **23**, 741–753 (2002).
4. L. O. Svaasand, L. T. Norvang, E. J. Fiskerstrand, E. K. S. Stopps, M. W. Berns, and J. S. Nelson, ''Tissue parameters determining the visual appearance of normal skin and port-wine stains,'' *Lasers Med. Sci.* **10**, 55–65 (1995).
5. L. F. A. Douven and G. W. Lucassen, ''Retrieval of optical properties of skin from measurement and modeling the diffuse reflectance,'' *Proc. SPIE* **3914**, 312–323 (2000).
6. W. Spalteholz, ''Die verteilung der blutge fäbe in der haut,'' *Arch. Anat. Physiol. Anat. Abt.* **2**, 1–54 (1893).
7. T. J. Ryan, ''Cutaneous circulation,'' Chap. 37 in *Physiology, Biochemistry, and Molecular Biology of the Skin*, vol 1, L. A. Goldsmith, Ed., pp. 1019–1084, Oxford Univ. Press, Oxford (1991).
8. M. J. C. Van Gemert, J. S. Nelson, T. E. Milner, D. J. Smithies, W. Verkruysse, J. F. de Boer, G. W. Lucassen, D. M. Goodman, B. S. Tanenbaum, L. T. Norvang, and L. O. Svaasand, ''Non-invasive determination of port wine stain anatomy and physiology for optimal laser treatment strategies,'' *Phys. Med. Biol.* **42**, 937–950 (1997).
9. S. H. Barsky, S. Rosen, D. E. Geer, and J. M. Noe, ''The nature and evolution of port wine stains: a computer-assisted study,'' *J. Invest. Dermatol.* **74**, 154–157 (1980).
10. W. F. Cheong, S. A. Prahl, and A. J. Welch, ''A review of the optical properties of biological tissues,'' *IEEE J. Quantum Electron.* **26**(12), 2166–2185 (1990).
11. S. J. Matcher, ''Signal quantification and localization in tissue near-infrared spectroscopy,'' Chap. 9 in *Handbook of Optical Biomedical Diagnostics*, V. V. Tuchin, Ed., SPIE Optical Engineering Press, Bellingham, WA (2002).
12. B. Hemmateenejad, R. Miri, M. Akhond, and M. Shamsipur, ''QSAR study of the calcium channel antagonist activity of some recently synthesized dihydropyridine derivatives: an application of genetic algorithm for variable selection in MLR and PLS methods,'' *Chemom. Intell. Lab. Syst.* **64**, 91–99 (2002).
13. T. J. Farrell, B. C. Wilson, and M. S. Patterson, ''The use of a neural

network to determine tissue optical properties from spatially resolved diffuse reflectance measurements,'' *Phys. Med. Biol.* **37**(12), 2281–2286 (1992).
14. W. Spendley, G. R. Hext, and F. Himsworth, ''Sequential application of simplex designs in optimization evolutionary operations,'' *Technometrics* **4**, 441–461 (1962).
15. J. Yen and B. Lee, ''A simplex genetic algorithm hybrid,'' *Proc. 1997 IEEE Intl. Conf. Evolutionary Computation*, pp. 175–180, New York (1997).
16. J. H. Holland, *Adaptation in Natural and Artificial Systems*, Univ. of Michigan Press, Ann Arbor, MI (1975).
17. D. A. Whitley, ''Genetic algorithm tutorial,'' *Stat. Comput.* **4**(2), 65–85 (1994).
18. L. Wang, S. L. Jacques, and L. Zheng, ''MCML—Monte Carlo modeling of light transport in multi-layered tissues,'' *Comput. Methods Programs Biomed.* **47**, 131–146 (1995).
19. J. Spanier and R. Kong, ''A new adaptive method for geometric convergence,'' *Proc. Monte Carlo Quasi-Monte Carlo Methods 2002*, H. Niederreiter, Ed., pp. 439–449, Springer-Verlag, Berlin, Germany (2004).
20. R. Kong and J. Spanier, ''Sequential correlated sampling methods for some transport problems,'' *Proc. Monte Carlo Quasi-Monte Carlo Methods 1998*, H. Niederreiter and J. Spanier, Eds., pp. 238–251, Springer-Verlag, Berlin, Germany (2000).
21. J. Spanier, ''Geometrically convergent learning algorithms for global solutions of transport problems,'' *Proc. Monte Carlo Quasi-Monte Carlo Methods 1998*, H. Niederreiter and J. Spanier, Eds., pp. 98–113, Springer-Verlag, Berlin, Germany (2000).
22. M. Keijzer, ''Light transport for medical laser treatments,'' PhD Thesis, Delft Univ. of Technology (1993).
23. K. S. Stenn, ''The skin,'' in *Cell and Tissue Biology*, L. Weiss, Ed., pp. 541–572, Urban and Shwarzenberg, Baltimore, MD (1988).
24. G. F. Odland, ''Structure of the skin,'' Chap. 1 in *Physiology, Biochemistry, and Molecular Biology of the Skin*, vol. 1, L. A. Goldsmith, Ed., pp. 3–62, Oxford Univ. Press, Oxford (1991).
25. K. A. Holbrook, ''Structure and functions of the developing human skin,'' Chap. 2 in *Physiology, Biochemistry, and Molecular Biology of the Skin*, vol. 1, L. A. Goldsmith, Ed., pp. 63–112, Oxford Univ. Press, Oxford (1991).
26. E. M. Renkin, C. C. Michel, and S. R. Geifer, ''The cardiovascular system,'' Sec. 2 in *Handbook of Physiology*. vol. 4, pts. 1 and 2, Mirocirculation, American Physiological Society, Bethesda, MD (1984).
27. S. L. Jacques, See http://omlc.ogi.edu/spectra/melanin/mua.html (1998).
28. L. T. Norvang, T. E. Milner, J. S. Nelson, M. W. Berns, and L. O. Svaasand, ''Skin pigmentation characterized by visible reflectance measurements,'' *Lasers Med. Sci.* **12**, 99–112 (1997).
29. O. Lakmaker, J. W. Pickering, and M. J. C. van Gemert, ''Modeling the color perception of port wine stains and its relation to the depth of laser coagulated blood vessels,'' *Lasers Surg. Med.* **13**, 219–226 (1993).
30. I. A. Niechajev and L. Clodius, ''Histology of port-wine stain,'' *Eur. J. Plast. Surg.* **13**, 79–85 (1990).
31. R. Zhang, see http://www.engr.ucr.edu/~gaguilar/RESEARCH.htm (2004).
32. D. J. Smithies, M. J. C. van Gemert, M. K. Hansen, T. E. Milner, and J. S. Nelson, ''Three-dimensional reconstruction of port wine stain vascular anatomy from serial histological sections,'' *Phys. Med. Biol.* **42**, 1843–1847 (1997).
33. W. Verkruysse, G. W. Lucassen, J. F. de Boer, D. J. Smithies, J. S. Nelson, and M. J. C. van Gemert, ''Modelling light distributions of homogeneous versus discrete absorbers in light irradiated turbid media,'' *Phys. Med. Biol.* **42**(1), 51–65 (1997).
34. E. J. Fiskerstrand, L. O. Svaasand, G. Kopstad, M. Dalaker, L. T. Norvang, and G. Volden, ''Laser treatment of port wine stains: therapeutic outcome in relation to morphological parameters,'' *Br. J. Dermatol.* **134**, 1039–1043 (1996).
35. J. A. Viator, J. Komadina, L. O. Svaasand, G. Aguilar, B. Choi, and J. S. Nelson, ''A comparative study of photoacoustic and reflectance methods for determination of epidermal melanin content,'' *J. Invest. Dermatol.* **122**, 1432–1439 (2004).
36. W. M. Star, ''Diffusion theory of light transport,'' Chap. 6 in *Optical-Thermal Response of Laser-Irradiated Tissue*, A. J. Welch and M. J. C. van Gemert, Eds., pp. 131–205, Plenum, New York (1995).
37. S. Prahl, see http://omlc.ogi.edu/spectra/hemoglobin/index.html (1999).
38. F. A. Duck, *Physical Properties of Tissue*, Academic Press, London (1990).
39. I. S. Saidi, *Transcutaneous Optical Measurement of Hyperbilirubinemia in Neonates*, PhD Thesis, Rice Univ., Houston, TX (1992).
40. S. L. Jacques, ''Origins of tissue optical properties in the UVA, visible and NR regions,'' in *Advances in Optical Imaging and Photon Migration*, vol. 2, R. R. Alfano and J. G. Fujimoto, Eds., pp. 364–370, OSA, Washington, DC (1996).